Composites Science and Technology 218 (2022) 109174

Contents lists available at ScienceDirect

Composites Science and Technology

journal homepage: www.elsevier.com/locate/compscitech

Development of hybrid steel-commingled composites CF/PEEK/BwM by filament winding and thermoforming

Ricardo Mello Di Benedetto [a,b,*], Anderson Janotti [b], Guilherme Ferreira Gomes [c], Antonio Carlos Ancelotti Junior [c], Edson Cocchieri Botelho [a]

[a] Materials and Technology Department, School of Engineering, São Paulo State University – UNESP, Av. Ariberto Pereira da Cunha, 333, Guaratinguetá, SP, Brazil
[b] Department of Materials Science & Engineering, University of Delaware – UDEL, 212 DuPont Hall, Newark, DE, USA
[c] Institute of Mechanical Engineering, Federal University of Itajubá – UNIFEI, Av. BPS, 1303, Itajubá, MG, NTC – Composite Technology Center, Brazil

ARTICLE INFO

Keywords:
Interlaminar shear properties
Structural composites
Thermomechanical analysis
Dynamic mechanical analysis
Metal-composite structure

ABSTRACT

A hybrid material made of carbon fiber, poly(ether-ether-ketone) and metallic braided wire mesh was designed to improve the crashworthiness of thermoplastic composite structures. The filament winding process was adapted to enable the winding of carbon fiber/poly(ether-ether-ketone) commingled tow with five different patterns of braided wire mesh, which were later consolidated by thermoforming. Samples of the hybrid steel-commingled composites were subjected to interlaminar shear strength tests, dynamic mechanical and thermo-mechanical analysis. Thermal analysis determined the glass transition, secondary temperature transitions, melting point, and the thermal expansion coefficient of CF/PEEK hybrid composites. The shear and thermal properties were investigated using statistical techniques of analysis of variance and design of experiments, highlighting the effects of the braided wire mesh parameters, i.e., mesh physical dimensions, on the material behavior. The incorporation of wire mesh showed no significant difference in the thermal properties of the hybrid composites and the applicability of these materials has no restrictive effect on temperature variations. An improvement of 22.7% in interlaminar shear strength was obtained for the hybrid metal-composite compared to the material without the braided wire mesh. Finally, a multiple regression model was developed to predict the interlaminar shear strength of hybrid steel-commingled composites as a function of the mesh parameters.

1. Introduction

Hybrid metal-composite structures (MCS) are being produced and constantly improved for automotive applications, aiming at reduced weight, and improved structural performance [1]. Thermoplastic composites (TPCs), in particular, have been used for multi-material structures due to the ability to be thermoformed, reducing throughput time. However, joining composites to metals has, until now, relied mostly on mechanical fasteners, which require drilling holes that damage load-bearing fibers, as evidenced by Nettles (2019) [2]. The drilling technique was evaluated by four different qualities of holes for fasteners. The author suggested visual inspection and thermography as inspection techniques to indicate the quality of the holes drilled in laminates. Adhesive bonding and chemical surface treatments have also been investigated, but thermoplastics materials are difficult to bond in this way. Marques et al. (2020) [3] realized that adhesives add material and weight to the structural components, and require proper chemical adhesion to steel-composites hybrid applicability.

In another recent study on multi-materials, by Yao et al. (2020) [4], the shear strength of steel-carbon fiber reinforced polymer (CFRP) hybrid composites was measured when the steel surfaces were treated with adhesive-bonding methods, abrasion and grit blasting. The results show the adhesion steel/CFRP has no significant effect on the mechanical properties of the hybrid composites. Crashworthiness of hybrid steel/carbon fiber composite was investigated by Kim et al. (2020) [5]. The study consisted of manufacturing a hybrid metal-composite automotive B-pillar component and comparing the results with a steel B-pillar. The performance of the composite structure increases when different materials are combined. This result indicates the effectiveness of the hybrid steel-composite combination for crashworthiness applications.

Mechanical properties of hybrid metal-composite carbon fiber (CF)

* Corresponding author. Materials and Technology Department, School of Engineering, São Paulo State University – UNESP, Av. Ariberto Pereira da Cunha, 333, Guaratinguetá, SP, Brazil.
E-mail address: ricardob@udel.edu (R.M. Di Benedetto).

https://doi.org/10.1016/j.compscitech.2021.109174
Received 24 June 2021; Received in revised form 27 September 2021; Accepted 19 November 2021
Available online 26 November 2021

reinforced polymer and stainless-steel wire mesh (SM) were evaluated by Truong and Choi (2021) [6]. Tensile tests were applied to the materials, which were composed of three different SM types and different CF orientations. An analytical model for predicting the load-strain curves of the hybrid composites was developed, showing good agreement with the experimental data. Krishnasamy et al. (2020) [7] evaluated the effect of aluminum (Al) and copper (Cu) wire mesh embedded as a structural reinforcement on epoxy hybrid composite. These studies focused on improving mechanical properties of composite structures, however, were limited to thermosetting resins to manufacture the composites, and do not include thermoplastics, which offer lower manufacturing costs and processing times [8,9]. Studies of hybrid composite materials that combine commingled technology and braided wire meshes with filament winding and thermoforming processes are scarce or inexistent in the literature.

The study of Rehra et al. (2018) [10] highlighted that the incorporation of steel fibers into carbon fiber reinforced polymer (CFRP) provides significant improvements of crashworthiness. The hybrid material post-damage performance depends on the laminate architecture, individual properties of the materials used and specially the interface adhesion [11]. The hybrid material interlaminar shear strength (ILSS) indicates the quality of interface bond when steel, reinforcing fibers and polymer are combined [12].

Automotive components are being manufactured using hybrid steel-composite technology. Gauntt and Campbell (2019) [13] created a hybrid steel-composite automotive gear with different materials and layups for rotorcraft industry. They evaluated the gear's resonance frequency for different configuration of hybrid materials. A model was developed based on the design of the gear and the materials properties. A B-pillar was designed and manufactured using CRFP hybrid steel-composite by Kim et al. (2020) [14]. Drop weight impact tests were conducted on the material considering the optimized stacking sequence, thickness, and shape for improving the crashworthiness. The CRPF hybrid steel-composite B-pillar resented improvement on the impact performance when compared with conventional steel B-pillar. These studies reveal the importance and relevance of developing new materials and processes for the manufacture of hybrid steel-composite components for automotive application.

This work reports the development of hybrid steel-composite carbon fiber/poly(ether-ether-ketone)/braided wire mesh (CF/PEEK/BwM) for crashworthiness improvement. BwM reinforced thermoplastic composites do not require adhesives or drilling holes for effective interface bond; the thermal consolidation is in itself responsible for compacting the material and subsequently impregnating the BwM with the thermoplastic polymer in the molten state. Processing parameters were defined according to the optimal response of PEEK[15,16], respecting thermal degradation limits during consolidation [17] obtained according to Friedman's isoconversional method [18]. A complete consolidation and higher matrix crystallization will result in higher interlaminar strength of the structure[19,20].

The design of the CF/PEEK/BwM steel-commingled hybrid composites has proven to be effective for structural application where crashworthiness is required. The adjustments in the filament winding process allowed manufacturing materials with high quality of compaction and processing control. Based on experimental data, a multiple regression model was developed to predict the ILSS of CF/PEEK/BwM with different combinations of BwM parameters, leading to the optimization of the structure performance.

2. Materials and methods

2.1. Steel-commingled hybrid composites manufacturing

This section describes the technical specifications of the materials and the stages of the hybrid composites design and manufacture. The CF/PEEK commingled tow was supplied by Concordia Manufacturing, LLC. The carbon fibers (CF) are characterized by 4240 MPa and 237 GPa of tensile strength and elastic modulus, respectively. The PEEK yarns have the specification PEEK-900/68, and the CF/PEEK commingled tow is classified as AS4 (40% matrix volume fraction) combining 12k carbon fiber tow with 7 μm diameter peek yarns.

Before the consolidation of the hybrid composites by thermoforming, the CF/PEEK commingled tow was subjected to a filament winding process with five different patterns of BwM. For this purpose, metal support was constructed to accommodate each BwM for the filament winding process. Fig. 1 represents the mechanism developed for the

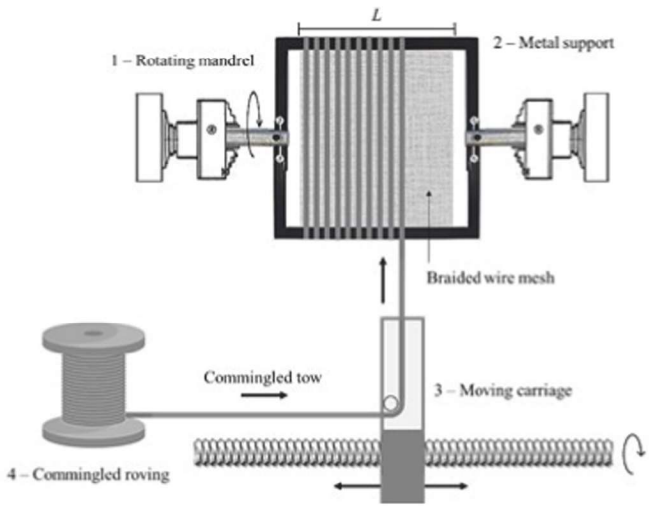

Fig. 1. Filament winding mechanism used to manufacture carbon fiber/poly (ether-ether-ketone)/braided wire mesh (CF/PEEK/BwM) hybrid composites.

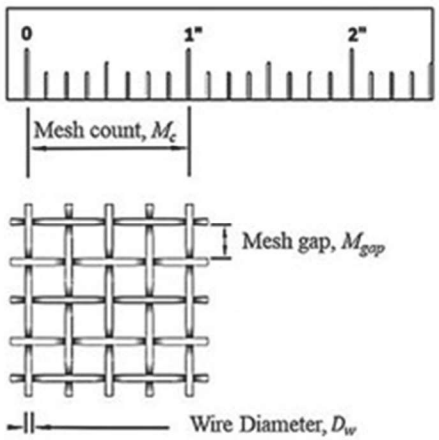

Fig. 2. Representation of braided wire mesh (BwM) pattern showing the physical dimensions used as parameters, which are mesh gap M_{gap}, wire diameter D_w, and mesh count M_c (M4 in this case).

Table 1
Summary of BwM patterns and the physical dimension used as parameters for each wire mesh used to manufacture CF/PEEK/BwM.

BwM	Mesh count, M_c	Wire diameter, D_w (mm)	Mesh gap, M_{gap} (mm)	Open area, A_{op} (%)	Area density, A_d (g/mm^2)
M14	14	0.30	1.51	69.6	0.07
M30	30	0.23	0.62	53.2	0.08
M40	40	0.20	0.44	47.2	0.08
M60	60	0.16	0.26	38.3	0.08
M80	80	0.12	0.20	39.0	0.07

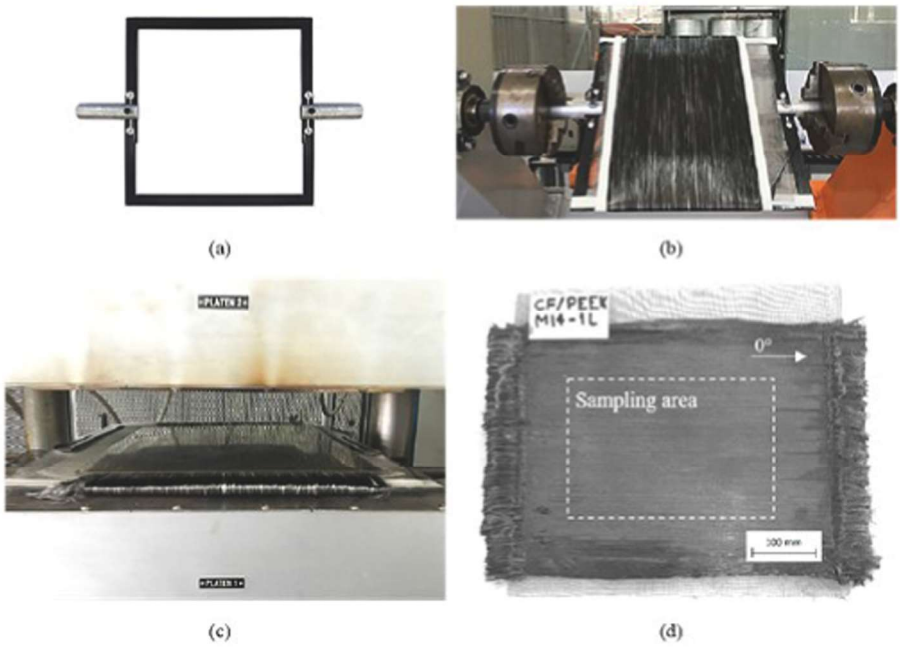

Fig. 3. Details of the CF/PEEK/BwM assembly and thermal consolidation processing. (a) The metal support used to wind the commingled yarn around the woven wire mesh. (b) CF/PEEK/BwM set after winding. (c) Steel plate used to ensure uniform load distribution in the material during thermal consolidation. (d) Final processed composite highlighting the sampling area.

assembly of CF/PEEK/BwM sets.

The rotating mandrel (1) pulls and wraps the CF/PEEK commingled tow around the BwM, which was first attached to the metal support (2). The winding cycles consist of moving the carriage (3) right and left (cycle) along the longitudinal length L. The commingled roving (4) feeds the filament winding process completing 5 cycles to each assembly composed by CF/PEEK commingled tow and BwM.

The BwM are made of stainless steel AISI 302 with linear coefficient of thermal expansion $\alpha = 17.6$ μm/m°C and elasticity modulus $E = 187.5$ GPa. The BwM were supplied by Catumbi Ltda. Five different patterns of BwM were used in this work. The physical parameters of a BwM pattern are shown in Fig. 2, and their values are listed in Table 1. The area density A_d is related to the hybrid composite weight gain. Mesh gap M_{gap} is the distance between the stainless-steel wires. Open area A_{op} represents the total percentage of the free area between the wires. The mesh count M_c is the wire mesh identification and related to the number of gaps within 1 inch distance.

A_{op} was used as an independent parameter because it refers to the contact area of the top and bottom layers during thermal consolidation. The values of A_{op} was used to investigate the effect of BwM incorpora-

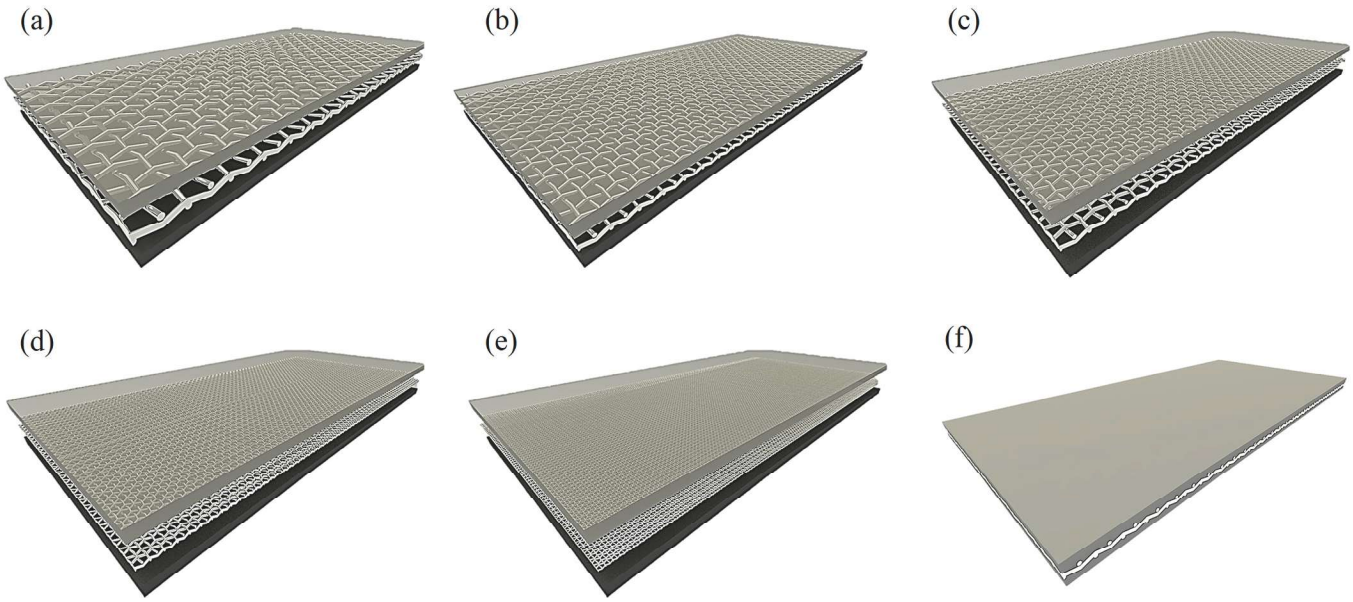

Fig. 4. Exploded-view drawings of CF/PEEK/BwM sets showing the assembly and dimensioning perspective of a 150 × 100mm sample: (a) CF/PEEK/BwM M14, (b) CF/PEEK/BwM M30, (c) CF/PEEK/BwM M40, (d) CF/PEEK/BwM M60, (e) CF/PEEK/BwM M80, and (f) representation of the hybrid steel-composite after thermal consolidation.

tion on the hybrid composites shear properties, and they were determined according to the Equation (1) [21],

$$A_{op} = \left(\frac{M_{gap}}{M_{gap} + D_w}\right)^2 x\ 100 \quad (1)$$

relating the mesh count M_c and the wire diameter D_w.

The construction of CF/PEEK/BwM sets, composed of commingled tow and BwM, required the production of machined metal support to fix the meshes for further filament winding processing. Fig. 3 shows (a) the metal support produced for the filament winding process; (b) the CF/PEEK/BwM set after winding; (c) the hydraulic press with heating system to consolidate the hybrid composite and (d) the CF/PEEK/BwM hybrid steel-composite.

Hybrid CF/PEEK/BwM steel-composites consist of multiple plies of commingled tow in the longitudinal direction (0°), in which the BwM defines the plane of symmetry. Carver hydraulic press model CMV100H-15-X was used to consolidate the hybrid composites with processing parameters given by Darcy's law, used to predict whether viscous fluid can impregnate the reinforcing fibers in a composite material [22]. The flow rate u_p of the viscous polymer can be calculated according to Equation (2). Taking $\frac{dP}{dx}$ constant, Equation (3) describes the impregnation time t_{imp} used to define the processing soak time:

$$u_p = \frac{dx}{dt} = \frac{K}{\nu}\frac{dP}{dx}, \quad (2)$$

$$t_{imp} = \frac{\nu D_p^2}{2KP}, \quad (3)$$

where ν is the polymer viscosity, K is the coefficient of permeability of the reinforcing fibers, $\frac{dP}{dx}$ is the pressure gradient, and D_p is the impregnation distance. The consolidation pressure $P = 0.3$ MPa was determined empirically in previous studies, as well as the matrix viscosity as a function of temperature [23]. Accordingly, the processing parameters were defined by $T_{processing} = 400$ °C, $t_{imp} = 20$min (holding time) using $\eta = 1000$ Pa s [24], $K = 1.4 \times 10^{-10}$ m^2[15,16,25,26], and $D_p = 0.3$ mm measured by the displacement of the hydraulic press plates. Final thickness ($e = 3.0 \pm 0.15$ mm) of the composites was defined according to the number of winding cycles (n = 5 cycles). Each winding cycle increase the hybrid material thickness in 0.6 mm because the mean of thickness of CF/PEEK tow is 0.3 mm. The range of the metallic wire diameter is 0.12–0.3 mm which causes a deviation ±0.15 mm for the final thickness of the hybrid composites. Thereby, the thermal processing cycle was defined with 5 °C/min of heating rate, 20 min of holding time (calculated by Eq. (3)) and 10 °C/min of cooling rate. The processing parameters are in accordance with the thermoplastic prepreg systems stablished by Takeda *el al.* (2019) [27], which contributes with the understand of the influence of cooling rate on the strength of composite materials. The quality of the hybrid composites considering total void elimination was achieved and confirmed with ultrasound inspection.

From the sampling area delimited in Fig. 3(d), specimens of CF/PEEK/BwM hybrid steel-commingled composites, labeled M14, M30, M40, M60 and M80, were prepared and subjected to ILSS tests, thermomechanical analysis (TMA) and dynamic mechanical analysis (DMA). Fig. 4 is a representation of the constituent layers of each hybrid composite.

2.2. ILSS tests

Shear properties of the CF/PEEK/BwM composites were evaluated by ILSS tests to examine the quality of the steel-matrix interface bonding for each BwM pattern. The universal testing machine EMIC DL2000A performed the ILSS tests with 1 mm/min of compression rate, 10 kN of load cell, 6 mm diameter loading nose, and 3 mm diameter supports consisting of the three-point flexure in accordance with ASTM 2344 standard. A total of 15 specimens (18 × 6x3mm) of each CF/PEEK/BwM composite were prepared and tested. The span length is 12 mm. Short-beam strength F^{sbs}, usually known as shear strength, is determined using a short beam shear test (SBS) and can be calculated by Equation (4) from ASTM 2344:

$$F^{sbs} = 0.75 \times \left(\frac{P_m}{b \times h}\right), \quad (4)$$

where P_m is the maximum load, b is the measured specimen width, and h is the measured specimen thickness.

2.3. Thermal analysis

Three specimens of each CF/PEEK/BwM were tested by DMA technique in an oxidative atmosphere to evaluate the material dynamic mechanical response as a function of temperature. Exstar SII 6000 equipment performed the tests with 1 Hz frequency, 33 μm amplitude, an oscillating load of 7000 mN, from 25 °C to 400 °C and heating rate $\frac{dT}{dt} = 10$ °C/min. Test conditions are in accordance with ASTM D7028. The idea is to verify the effect of BwM incorporation on glass transition temperature T_g, secondary transition temperature T_α^*, and melt temperature T_m of the hybrid steel-composites by evaluating elastic modulus (or storage modulus, E'), viscous modulus (or loss modulus, E″) and damping coefficient (Tan δ). The peaks observed on E" curve is related to T_g, T_α^* and T_m, respectively [28].

The TMA was performed by SII EXSTAR 6000 equipment, in three samples for each CF/PEEK/BwM, in an oxidative atmosphere from 25 °C to 400 °C with a heating rate $\frac{dT}{dt} = 5$ °C/min, and constant load of 100 mN. TMA was conducted according to the ASTM E831 to measure linear coefficients of thermal expansion (α) of CF/PEEK/BwM hybrid steel-composites. TMA measured the temperature-dependent dimensional changes while allowing the specimens of CF/PEEK/BwM to be subjected to mechanical load. This makes it possible to determine the thermal length change as well as the thermomechanical characteristics of the hybrid steel-composites developed. Linear coefficients of thermal expansion α is essential for assessing the dimension changes as function of temperature for different BwM patterns of the hybrid composites. The mean coefficient of linear thermal expansion ($\overline{\alpha}$) is defined as the slope of a secant through two points of the curve of thermal expansion (Equation (5)):

$$\overline{\alpha} = \frac{\Delta L_{sp} \times k}{L \times \Delta T}, \quad (5)$$

where k is calibration of the length change (deflection), L is the calibration length, ΔL_{sp} is the change of specimen length, and ΔT is the temperature difference over which the change in specimen length is measured.

2.4. Statistics and data analysis

The experimental results were subjected to analysis of variance (ANOVA), design of experiments (DOE), and multiple linear regression (MLR). In its simplest form, ANOVA provided a preliminary statistical test on the database, comparing means of thermomechanical properties and of shear strength measured. Subsequently, DOE described and explained the variation of the material behavior as a function of BwM patterns. A full factorial design evaluated main effects and significant interactions between independent variables. Finally, MLR determined a model that considers the relations between BwM patterns, polymer thermal properties and $\overline{\alpha}$ to predict the CF/PEEK/BwM shear strength.

Minitab software resources performed the ANOVA and DOE analyzes. The MLR was created by an integrated development environment for *R* programming language for statistical computing [17,18]. To

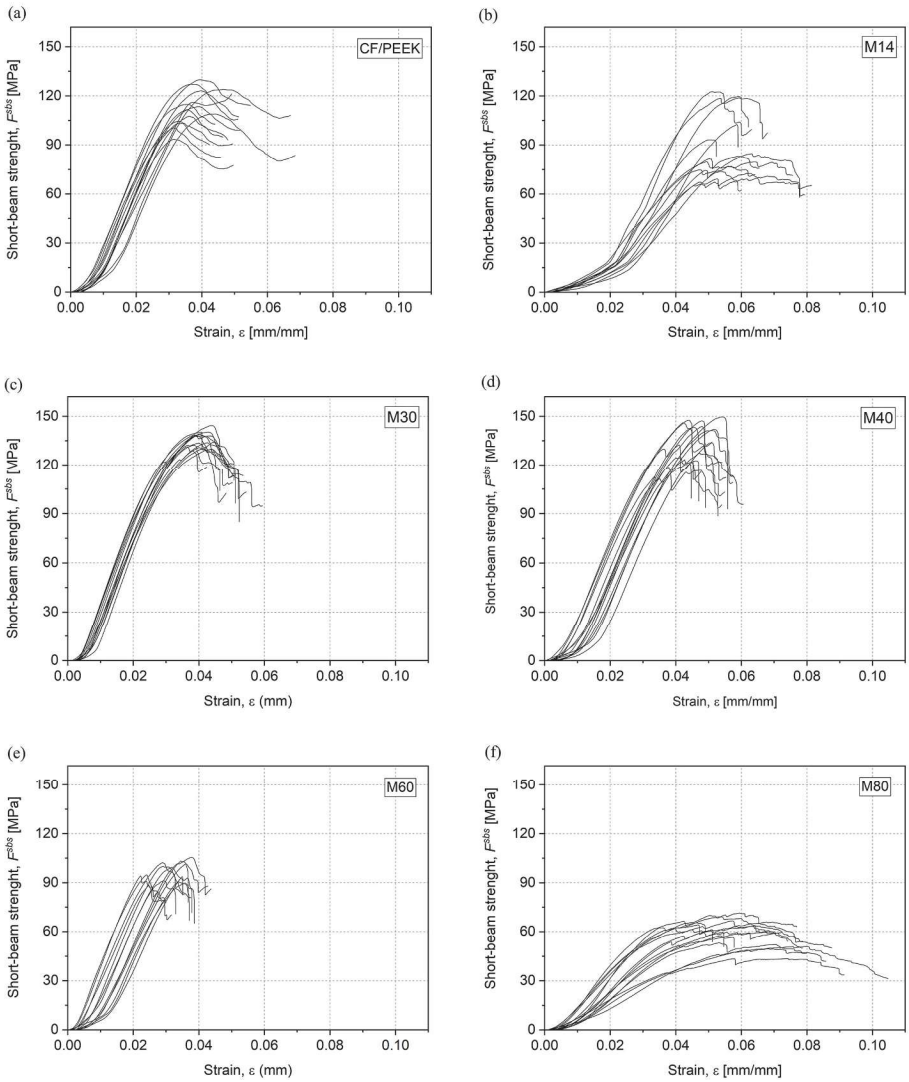

Fig. 5. Short-beam strength *versus* strain plots for ILSS tests of CF/PEEK composite and CF/PEEK/BwM M14, M30, M40, M60 and M80 steel-commingled hybrid composites.

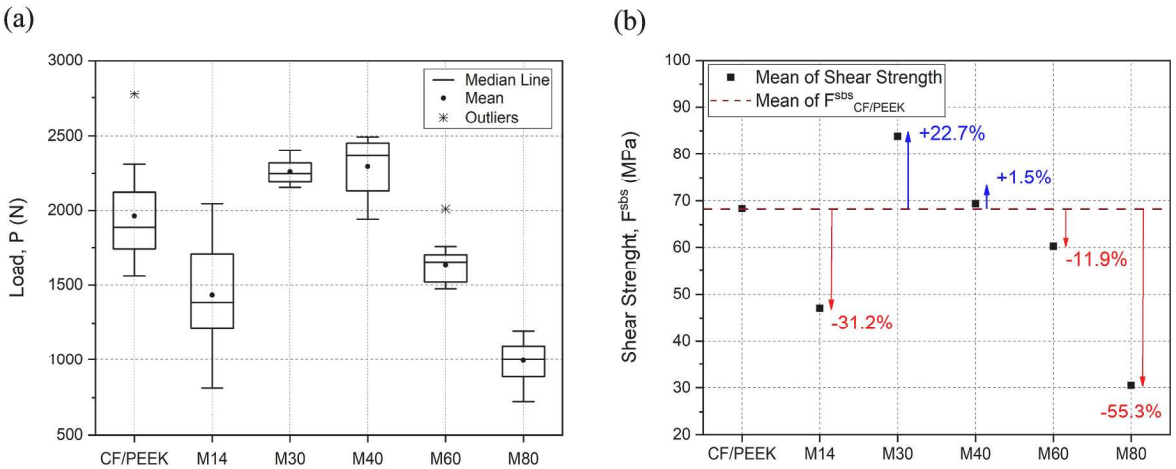

Fig. 6. Compilation of the ILSS test results. (a) Boxplot of maximum load showing intervals, means and outliers. (b) Shear strength of tested materials and the percentual difference compared to CF/PEEK standard.

Table 2
Results of ILSS tests for CF/PEEK and CF/PEEK/BwM ILSS hybrid composites. Outlier data for CF/PEEK and M60 were not included.

Material	Number of samples	Mean of maximum load (N)	Standard deviation of maximum load (N)	Short-beam strength (MPa)
CF/PEEK	14	1905.90	211.27	68.35
M14	15	1435.00	367.49	47.04
M30	15	2260.20	75.96	83.86
M40	15	2294.20	182.89	69.37
M60	14	1611.30	92.69	60.23
M80	15	993.65	128.94	30.51

determine a more appropriate fit for the data, the method of least square was used to minimize the maximum likelihood function L of the model (Eq. (6)) [29,30]. The function L measures the probability of observing the set of dependent variable values; the higher the likelihood function L, the higher the probability of observing the dependent variable values in the sample [31], as in Equation (6):

$$L = \sum_{i=1}^{n} \left(Y_i - \beta_0 + \beta_1 x_{i1} + \beta_2 x_{i2} + \ldots + \beta_p x_{ip}\right)^2. \quad (6)$$

The regression coefficients β_i indicate a change in the mean response of F^{sbs} according to the independent variable x_i when the other variables are kept fixed. Y_i is the response-dependent variable F^{sbs}. Subsequently, the stepwise method of variable selection determined a subset of independent variables that best estimate F^{sbs}. Subsequently, the Akaike Information Criterion (AIC) was based on sample fit to estimate the likelihood of the MLR model to predict F^{sbs}. The minimum value of AIC calculated by Equation (7) defines the variables which were included on the model [32]:

$$AIC = -2log\left(L_p\right) + 2[(p+1)+1], \quad (7)$$

where L_p is the maximum likelihood function of MLR model and p is the number of explanatory variables.

3. Results

3.1. Shear properties of steel-commingled hybrid composites

The ILSS tests were applied to CF/PEEK composite, and the M14, M30, M40, M60 and M80 steel-commingled hybrid composites. Graphical ILSS results are shown in Fig. 5. The results show changes in the mechanical responses of CF/PEEK/BwM hybrid composites for each BwM pattern, keeping both processing parameters and the number of winding cycles the same for all specimens. Understanding the effects of BwM patterns parameters D_w, M_g and A_{op} on the shear strength aims to optimize crashworthiness of CF/PEEK/BwM hybrid composites. The non-uniformity of the mechanical behavior regarding M14 and M80 samples is associated with a premature detachment at the interface metal/polymer, which occurs at the beginning of displacement. Depending on the position of the BmW within the material and the sampling cut, premature detachment can happen more easily in these configurations. This can be confirmed by evaluating the strain values of ILSS tests and also by the results obtained by Wu et al. (2014), who used scanning electron microscopy (SEM) to investigate the fracture mechanism [33].

From Fig. 5, it is clear that the differences in mechanical behavior of these materials are related to the effects of BwM incorporation. Next, Fig. 6 summarizes (a) the mean values of P_m and (b) the mean of shear strength F^{sbs}, calculated according to Eq. (4).

The boxplot in Fig. 6(a) shows the distribution of P_m of the composites. Basically, M14 presented higher dispersion of P_m values and M30 presented the lowest dispersion. The CF/PEEK, M40, M60, and M80 presented similar dispersion of P_m. Only two outliers were identified within the total sampling amount, one for CF/PEEK and the other for M60, as seen in Fig. 6(a). Samples of the same material can have different numbers of nodes (wire over wire), depending on how the sampling was prepared. Accordingly, CF/PEEK/BwM presented different means of P_m.

Fig. 6(b) shows the shear strength F^{sbs} of CF/PEEK/BwM steel-commingled hybrid composites and CF/PEEK for comparison. The percentual related to the difference between F^{sbs} of the CF/PEEK/BwM hybrid composites and CF/PEEK are indicated. M14, M60 and M80 decreased F^{sbs} by 31.2%, 11.9% and 55.3%, respectively. M40 almost kept the same F^{sbs} of CF/PEEK, just 1.5% higher. The mechanical performance of CF/PEEK/BwM M30 overmatch other specimens. It displays F^{sbs} 22.7% higher than CF/PEEK. Table 2 summarizes the results obtained from the ILSS tests.

Although the ILSS test results for short-beam strength are quite apparent, the results of statistical analysis are more precise to describe whether these improvements of mechanical behavior are significant or not. The statistical analysis was also used to verify the effects of D_w and A_{op} on ILSS. Differences between the mean of P and F^{sbs} were assessed using ANOVA, removing the outlier points, the results of which are listed in Table 3.

Table 3
Analysis of variance of maximum load means between all the composites.

Source	DF	Adj SS	Adj MS	F-Value	P-Value
Factor	5	19015973	3805195	92.74	0.001
Error	82	3364516	41031		
Total	87	22390489			

Table 4
Analysis of variance of maximum load to compare the mean of CF/PEEK and the M30 sample.

Source	DF	Adj SS	Adj MS	F-Value	P-Value
Factor	1	908555	908555	37.11	0.001
Error	27	661051	24483		
Total	28	1569606			

P-Value less than the level of significance of 0.05 indicates that differences between the means of P_m are statistically significant and, therefore, the shear properties of CF/PEEK/BwM steel-commingled hybrid composites are indeed affected by D_w and A_{op}. Due to the performance of CF/PEEK/BwM M30, the results were compared with those of CF/PEEK by the two-factor ANOVA method. P-Value < 0.05 revealed a significant difference between the means of P_m and it proves the improvement of the structure performance. Therefore, the incorporation of BwM in thermoplastic composites can be successful if it respects the best combination of D_w and A_{op}. Table 4 shows the two-factor ANOVA analysis results.

The effects of D_w, A_{op} and the interaction $D_w{*}A_{op}$ on the shear properties of CF/PEEK/BwM were evaluated by DOE technique, and the results placed in descending order according to the Pareto chart shown in Fig. 7(a). The results of the statistical analysis summarized in Table 5 clearly show the influence of BwM patterns on the shear properties of CF/PEEK/BwM. Standardized effects above the reference line at 4.30 means the factors significantly affect the shear properties of CF/PEEK/BwM hybrid steel-commingled composites. Fig. 7(b) shows the contour plot of the ILSS test results, showing the changes on the material shear property as a function of D_w and A_{op}.

The Pareto chart reveals that not only D_w and A_{op}, but also the product $D_w{*}A_{op}$ has a significant effect on the ILSS of CF/PEEK/BwM. Adding interaction terms to the MRL model contributes to the understanding of the relationships between variables and allows more hypotheses to be tested. The presence of significant interaction indicates that the effect of one predictor variable on the response variable is

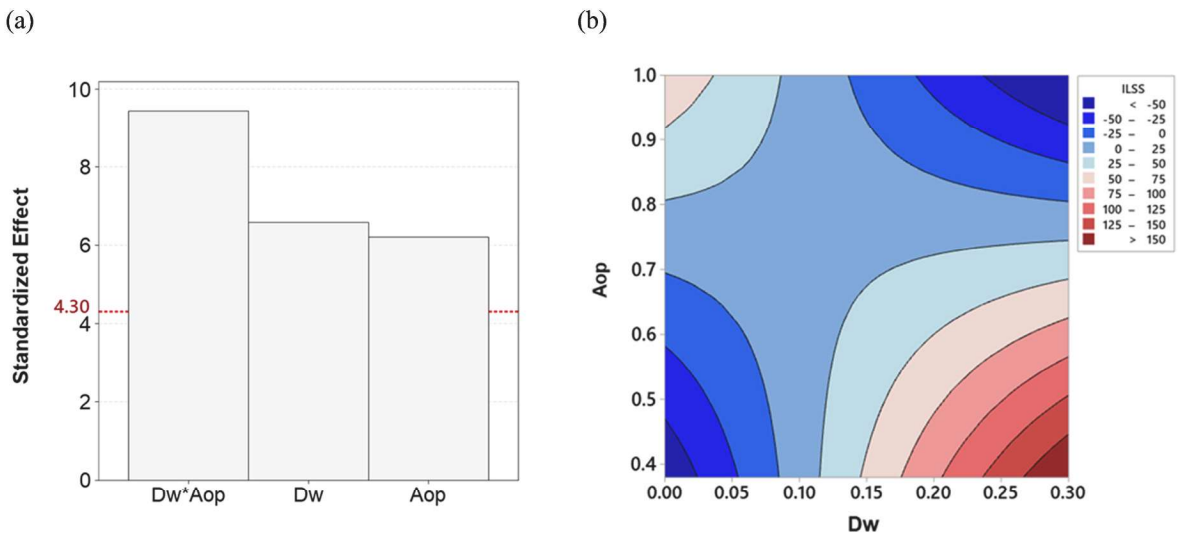

Fig. 7. DOE graphics to illustrate the relation between the factors D_w, A_{op} and D_w*A_{op}. (a) Pareto chart for ILSS. (b) Contour plot for ILSS test results.

Table 5
Coded coefficients and P-Values of the full factorial design.

Factor	Effect	Coefficient of variation	SE Coefficient of variation	T-Value	P-Value
Constant		23.43	4.54	5.16	0.036
D_w	48.88	24.44	3.71	6.58	0.022
A_{op}	−60.63	−30.31	4.88	−6.21	0.025
D_w* A_{op}	−199.4	−99.7	10.6	−9.45	0.011

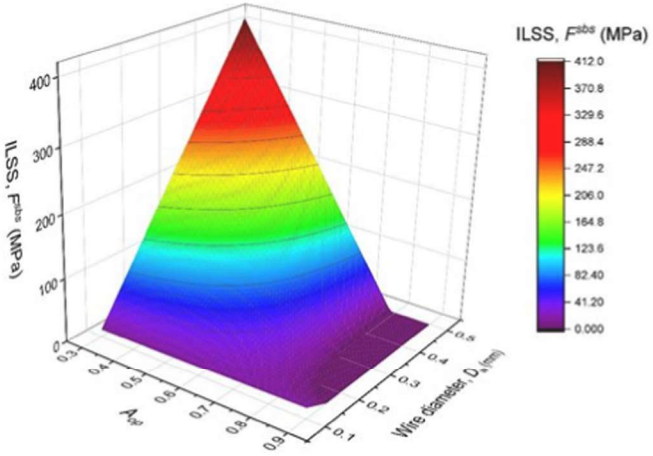

Fig. 8. 3D Surface response plot for CF/PEEK/BwM ILSS based on MRL model.

different at different values of the other predictor variable. It is tested by adding a term to the model in which the two predictor variables are multiplied. The MLR model predicts ILSS of CF/PEEK/BwM as a function of D_w, A_{op} and D_w*A_{op}, as described by Equation (8).

$$ILSS = \beta_0 + \beta_1 \times D_w + \beta_2 \times A_{op} + \beta_3 \times D_w{}^*A_{op}. \quad (8)$$

Here, β_0, β_1,β_2 and β_3 are the regression coefficients, respectively, with values of −155.5, 1643, 223.9 and −2145. The model presents a coefficient of determination R^2_{adj} = 0.9501 and it properly fits the experimental data.

The response surface methodology (RSM) was helpful in graphically indicating predictable values of ILSS for different combinations of D_w and A_{op}, providing an overview of CF/PEEK/BwM hybrid composites shear properties. Fig. 8 shows the surface response of ILSS for the hybrid composite materials.

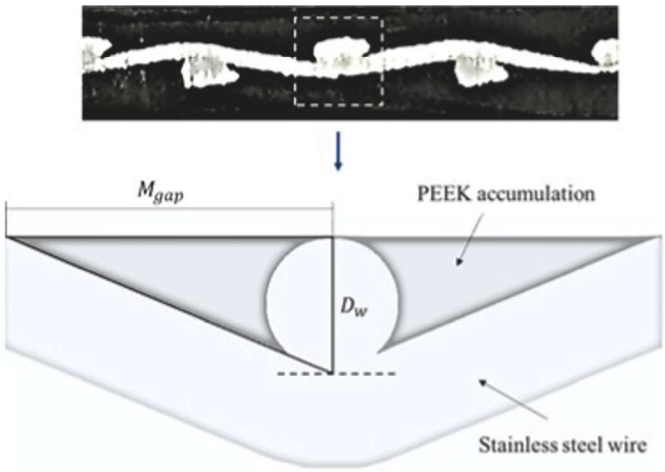

Fig. 9. CF/PEEK/BwM cross-section showing the zone of polymer accumulation promoting mechanical anchoring mechanisms.

Higher values of ILSS are found for the combination of D_w, from 0.4 to 0.5 mm, and A_{op} from 0.3 to 0.4 and confirm that the interaction of these variables has significant effect on the material shear properties. Therefore, the shear properties of CF/PEEK/BwM are optimized increasing D_w and reducing A_{op}. Another relevant aspect is the linearity seen in the relationship between these two factors when ILSS increases. It proves the significant effect of the interaction D_w*A_{op} on shear properties of CF/PEEK/BwM composites. This effect is intensified when A_{op} increases and D_w decreases, simultaneously.

Changes in the shear properties are attributed to the mechanical anchoring between BwM and the polymer. During thermoforming, A_{op} is filled just by the PEEK in the molten state. Due to the geometry of BwM, the carbon fibers just act on its faces, but not within the braided mesh. Fig. 9 shows the CF/PEEK/BwM cross-section and the representation of the PEEK accumulation region. The region of PEEK accumulation is directly related to D_w. As previously demonstrated by statistical analysis, higher values of D_w increase the ILSS. This is due to the mechanical anchoring that is most effective when D_w is greater, creating a blockage of the shear movement. In addition, lower M_{gap} values mean more wires

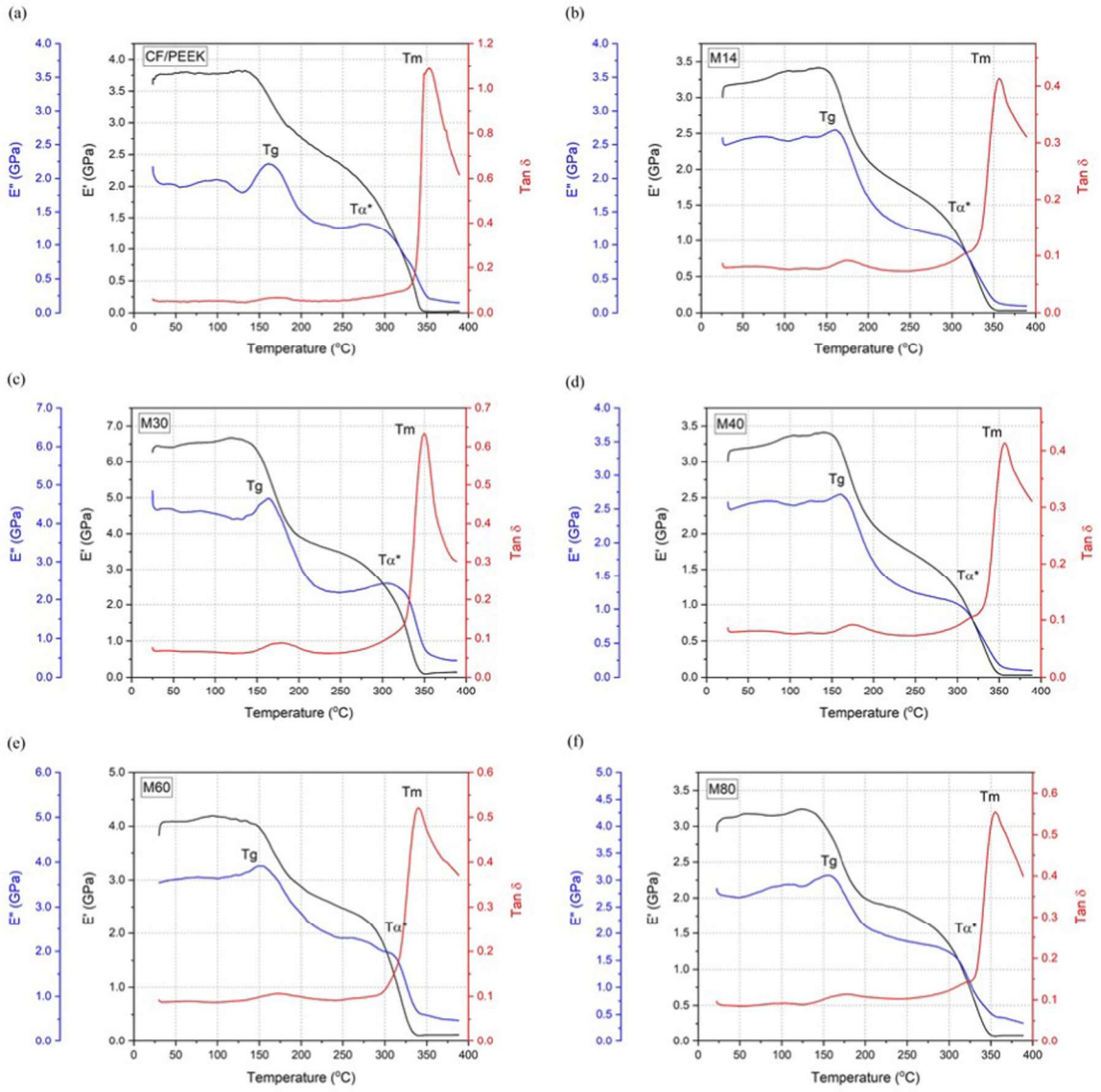

Fig. 10. Dynamic mechanical analysis (DMA) thermograms showing the behavior of the CF/PEEK/BwM hybrid composites (M14, M30, M40, M60, and M80), compared to that of CF/PEEK.

in the BwM patterns per unit area, translating into more mechanical anchoring points providing CF/PEEK/BwM shear properties improvement.

3.2. Dynamic mechanical analysis

The material characterization by DMA identified viscoelastic behavior of the polymeric matrix while it is subjected to a temperature regime. A sinusoidal stress was applied to measure the material strain, allowing one to determine the complex modulus *E'*, *E''* and *Tan δ*. The temperature of the sample or the frequency of the stress are often varied, leading to variations in the complex modulus; this approach can be used to locate the glass transition temperature T_g of the material, as well as to identify transitions corresponding to other molecular motions as T_α^* and melting point T_m. Fig. 10 contains the DMA thermograms for CF/PEEK and CF/PEEK/BwM hybrid composites (see Fig. 11).

An ideal type of DMA thermograms due to T_g values are clearly displayed in Fig. 10. In the region of the glass transition molecular segmental motions are activated, however motions occur with difficulty, described as molecular friction that dissipates much of the force. Therefore, though the material reduces its stiffness, more force is dissipated as heat, increasing the loss modulus. This is an alternative definition of T_g such as the peak of the loss modulus.

According to the DMA, mean of T_g of 159 ± 4 °C, and mean of T_m of 352 ± 6 °C were obtained. Low values of standard deviation indicate that BwM incorporation does not affect the polymer thermal behavior. However, when evaluating secondary transition T_α^*, a change in the baseline was observed for CF/PEEK/BwM. This change can be considered an effect of the thermal conductivity of stainless steel, not exactly a change in the thermal properties. T_α^* is associated with conformational changes in molecular rearrangements and can be affected by the difference between the thermal conductivity of stainless steel (14 W/m.K) and PEEK (0.24 W/m.K). Thermal conductivity quantifies the ability of materials to conduct thermal energy. The metal structure conducts thermal energy more quickly and efficiently than PEEK, especially when the polymer is in the molten state. However, part of the thermal energy is absorbed by the BwM which explains why the higher temperatures of secondary transitions are observed for CF/PEEK/BwM.

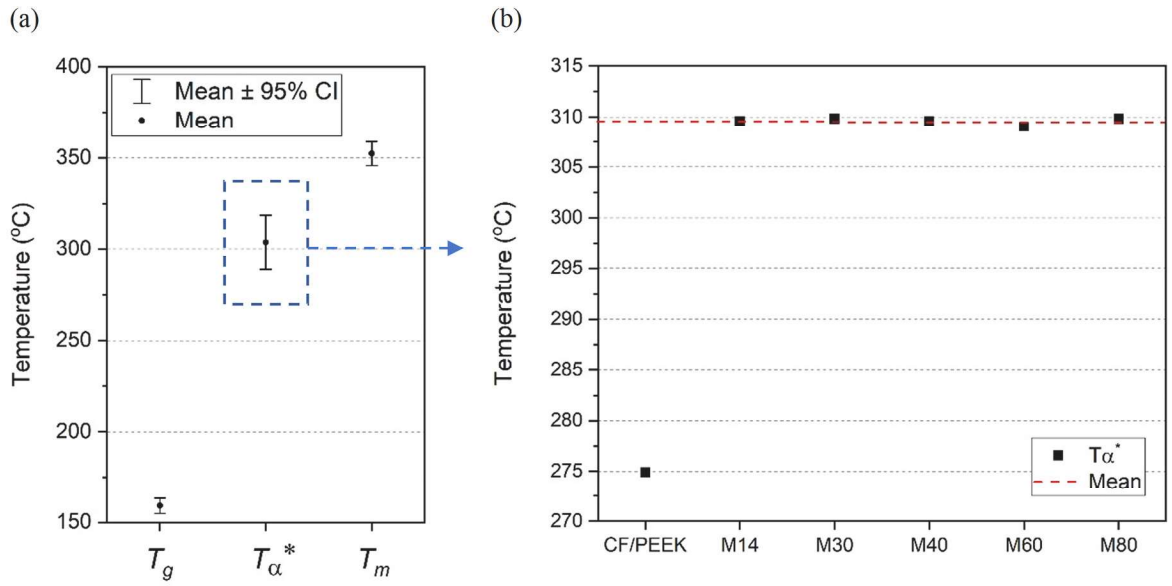

Fig. 11. Interval plot for DMA results. (a) Thermal properties of the composites. (b) Detailing of T_α^* values showing the difference of CF/PEEK and CF/PEEK/BwM.

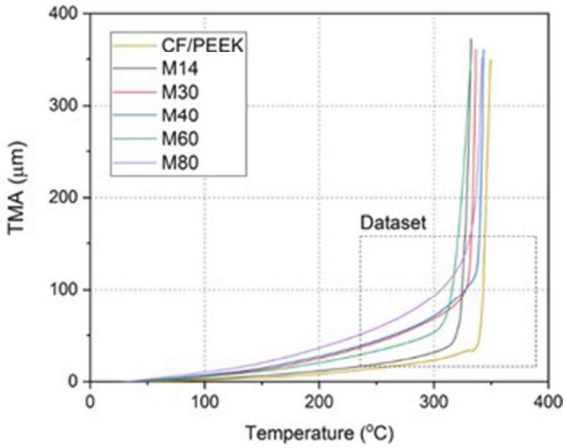

Fig. 12. Area of interesting of TMA plot to determine $\overline{\alpha}$ of CF/PEEK/BwM hybrid composites according to ASTM E831.

Table 6
Summary of TMA results for CF/PEEK and CF/PEEK/BwM.

Specimen	ΔL (µm)	T_{onset} (°C)	T_{end} (°C)	$\overline{\alpha}$ (µm/m°C)
CF/PEEK	40	335	345	14
M14	40	315	330	13
M30	100	328	336	26
M40	110	336	342	25
M60	50	300	325	7
M80	120	327	340	12
Mean	77	324	336	16
Standard deviation	37	14	8	8

3.3. Thermomechanical analysis

TMA analysis allowed the monitoring of CF/PEEK/BwM thermal expansion while a compressive force was applied to the material. The technique was used to investigate the influence of BwM addition on the linear coefficient of thermal expansion α of the hybrid composites. The thermal expansion was measured within the limits of temperatures T_{onset} and T_{end} of each specimen. Note that the determination of the measurement limit was based on changes of the response curve where the dataset was located, as shown in Fig. 12. The summary of the TMA results are listed in Table 6, and can be visualized in Fig. 13, with individual plots for CF/PEEK, and M30, M40, M60 and M80 hybrid composite samples.

The differences observed on $\overline{\alpha}$ were statically evaluated by factorial regression. P-Values $>$ 0.05 means a non-significant difference was observed within the specimens. Therefore, $\overline{\alpha}$ is not affected by BwM incorporation and it does not depend on D_w, A_{op} and the interaction $D_w{*}A_{op}$. Table 7 summarizes the analysis of variance coefficients.

4. Conclusions

The filament winding process was completely adjusted to construct the CF/PEEK/BwM set. The mandrel rotation is the impeller to construct the steel-commingled preform, in which no other tow tensioning system was required. The mechanism proposed can also be used to construct different types of steel-commingled hybrid sets based on the number of BwM layers and its settings. The final thickness of the hybrid composites can be adjusted according to the number of winding cycles and the diameter of the wires.

The shear properties of CF/PEEK/BwM hybrid steel-commingled composites depend on wire diameter and the open area between the wires. However, the higher effect on shear properties is related to the interaction of these two parameters. Although there are conditions in which BwM incorporation increases shear strength of the composites, the mechanical response optimization depends mainly on the interaction effects between wire diameter and open area. Mechanical anchoring points are responsible for increasing tension level before the detachment on an interface, which increases interlaminar shear strength. The optimized response indicates the best fit between wire diameter and open area to increase shear properties of CF/PEEK/BwM steel-commingled hybrid composites.

In order to correlate the shear behavior of the steel-commingled hybrid composites with BwM parameters, a multiple regression method has been used. The regression model can predict interlaminar shear strength of CF/PEEK/BwM according to different wire diameter and open area. Understanding the shear behavior can bring benefits to the crashworthiness of composite materials and make them more efficient in a collision event. This study also has important applications in

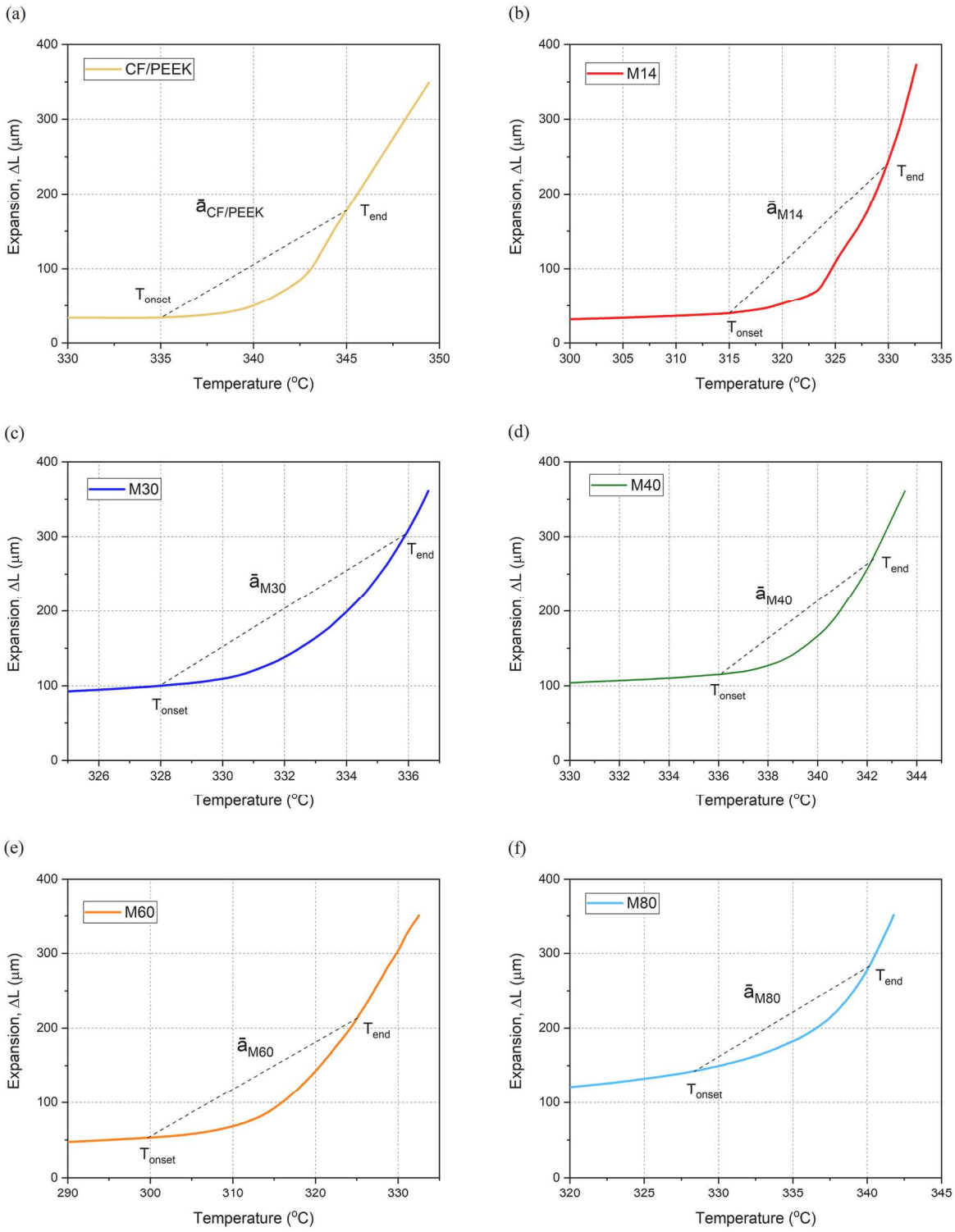

Fig. 13. Results of thermomechanical analysis (TMA) for CF/PEEK and CF/PEEK/BwM to determine the coefficient of linear expansion α.

the design, development, and formulation of hybrid structures, as well as in the improvement of existing product designs as B-pillar, inner door panel, anti-collision side door beam and bumpers.

Author statement

The authors assume responsibility for the content of the work submitted for review. The contributions of all referees were considered and carefully reviewed. Contributions from referees have improved the quality of the work, and we are grateful for that.

The authors thank the editorial board for providing us with the opportunity to respond to reviewer comments and resubmit our working title "DEVELOPMENT OF CF/PEEK/BwM HYBRID COMINGLED STEEL COMPOSITES BY FILAMENT WINDING AND THERMOFORMING".

This work presents the development of a new hybrid composite steel material that has applicability for engineering. The content of this study is innovative and can be used in future work. We look forward to publishing this manuscript in the prestigious journal of COMPOSITES

Table 7
Analysis of variance results from the factorial regression design.

Source	DF	Adj SS	Adj MS	F-Value	P-Value
Model	3	148.94	49.65	0.70	0.634
Linear	2	138.23	69.11	0.97	0.507
$\varnothing_w$	1	109.47	109.47	1.54	0.340
A_{op}	1	58.66	58.66	0.83	0.459
2-Way Interactions	1	122.12	122.12	1.72	0.320
$\varnothing_w * A_{op}$	1	122.12	122.12	1.72	0.320
Error	2	141.89	70.94		
Total	5	290.83			

SCIENCE AND TECHNOLOGY.

Declaration of competing interest

The authors declare that they have no known competing financial interests or personal relationships that could have appeared to influence the work reported in this paper.

Acknowledgments

The authors acknowledge the financial support from FAPESP (São Paulo Research Foundation) under projects 2019/22173-0, 2018/24964-2 and 2017/16970-0; from CNPq (National Council for Scientific and Technological Development) under project 306576/2020-1, 311709/2017-6 and 307446/2020-4; from FINEP project number 0.1.13.0169.00 and FAPEMIG (research supporting foundation of Minas Gerais state – Grant number APQ-00385-18 and APQ-01846-18). AJ acknowledges support from NSF Early Career Award grant number DMR-1652994. The authors would like to thank the Composite Technology Center (NTC) from Federal University de Itajubá-Brazil for the general facilities.

References

[1] E. Hannemann, S. Backe, S. Schemeer, F. Balle, U.P. Breuer, J. Schuster, Hybridisation of CFRP by the use of continuous metal fibres (MCFRP) for damage tolerant and electrically conductive lightweight structures, Compos. Struct. 172 (2017) 374–382, https://doi.org/10.1016/j.compstruct.2017.03.064.
[2] A.T. Nettles, The effect of hole quality on the bearing strength of carbon fiber laminates. https://ntrs.nasa.gov/api/citations/20190027642/downloads/20190027642.pdf, 2019.
[3] A.C. Marques, A. Mocanu, N.Z. Tomic, S. Balos, E. Stammen, A. Lundevall, S. T. Abrahami, R. Gunther, J.M.M. Kok, S.T. Freitas, Review on adhesives and surface treatments for structural applications: recent developments on sustainability and implementation for metal and composite substrates, Materials 13 (2020) 5590, https://doi.org/10.3390/ma13245590.
[4] Y. Yao, P. Shi, S. Qi, C. Yan, G. Chen, D. Liu, Y. Zhu, A. Herrmann, Manufacturing and mechanical properties of steel-CFRP hybrid composites, J. Compos. Mater. 54 (2020) 3673–3682, https://doi.org/10.1177/0021998320918287.
[5] D. Kim, J. Lim, B. Nam, H.J. Kim, H.S. Kim, Design and manufacture of automotive hybrid steel/carbon fiber composite B-pillar component with high crashworthiness, J. Precis. Eng. Manuf. 8 (2020) 547–559, https://doi.org/10.1007/s40684-020-00188-5.
[6] G.T. Truong, K. Choi, Tensile behavior of hybrid composites of carbon fibers-steel wire mesh reinforced polymer, Mech. Adv. Mater. Struct. 28 (2021) 154–166, https://doi.org/10.1080/15376494.2018.1553256.
[7] M. Krishnasamy, P. Rajamurugan, G. Thirumurugan, Performance of fiber metal laminate composites embedded with AL and CU wire mesh, J. Ind. Textil. 1 (2020) 1–18, https://doi.org/10.1177/1528083720935570.
[8] R.M. Di Benedetto, E.C. Botelho, G.F. Gomes, D.M. Junqueira, A.C. Ancelotti Junior, Impact energy absorption capability of thermoplastic commingled composites, Compos. B Eng. 176 (2019) 1–29, https://doi.org/10.1016/j.compositesb.2019.107307.
[9] R.M. Di Benedetto, E.C. Botelho, A. Janotti, A.C. Ancelotti Junior, G.F. Gomes, Development of an artificial neural network for predicting energy absorption capability of thermoplastic commingled composites, Compos. Struct. 257 (2021) 113–131, https://doi.org/10.1016/j.compstruct.2020.113131.
[10] J. Rehra, B. Hannemann, S. Schemeer, J. Hausmann, P. Breuer, Approach for an analytical description of the failure evolution of continuous steel and carbon fiber hybrid composites, Adv. Eng. Mater. 21 (2018) 1800565, https://doi.org/10.1002/adem.201800565.
[11] S. Schmeer, M. Steeg, M. Maier, P. Mitschang, Metal fibre reinforced composite – potentialities and tasks, Adv. Compos. Lett. 18 (2009) 45–52, https://doi.org/10.1177/096369350901800202.
[12] P. Krishnam, Mechanical and physical testing of biocomposites, fibre-reinforced composites and hybrid composites, Woodhead Publ. Ser. Compos. Sci. Eng. 1 (2019) 343–385, https://doi.org/10.1016/B978-0-08-102292-4.00018-7.
[13] S.M. Gauntt, R.L. Cambell, in: Characterization of a Hybrid (Steel-Composite) Gear with Various Composite Materials and Layups, AIAA SciTech Forum, 2019, pp. 1–9.
[14] D.J. Kim, J. Lim, B. Nam, H.J. Kim, H.S. Kim, Design and manufacture of automotive hybrid steel/carbon fiber composite B-pillar component with high crashworthiness, Int. J. Precis. Eng. Manuf. Technol. 8 (2020) 547–559, https://doi.org/10.1007/s40684-020-00188-5.
[15] L. Pan, U. Yapici, A comparative study on mechanical properties of carbon fiber/PEEK composites, Adv. Compos. Mater. 25 (2016) 359–374, https://doi.org/10.1080/09243046.2014.996961.
[16] A.R. McLauchlin, O.R. Ghita, L. Savage, Studies on the reprocessability of poly (ether ether ketone) (PEEK), J. Mater. Process. Technol. 214 (2014) 75–80, https://doi.org/10.1016/j.jmatprotec.2013.07.010.
[17] A. Pascual, M. Toma, P. Tsotra, M.C. Grob, On the stability of PEEK for short processing cycles at high temperatures and oxygen-containing atmosphere, Polym. Degrad. Stabil. 165 (2019) 161–169, https://doi.org/10.1016/j.polymdegradstab.2019.04.025.
[18] H.L. Friedman, Kinetics of thermal degradation of char-forming plastics from thermogravimetry, J. Polym. Sci., Polym. Symp. 6 (1964) 183–195, https://doi.org/10.1002/polc.5070060121.
[19] D. Saenz-Castillo, M.I. Martin, S. Calvo, A. Guemes, Real-time monitoring of thermal history of thermoplastic automatic lamination with FBG sensors and process modelling validation, Smart Mater. Struct. 29 (2020) 1–35, https://doi.org/10.1088/1361-665X/abaa97.
[20] I. Martin, D.S. Castillo, A. Fernandez, A. Guemes, Advanced thermoplastic composite manufacturing by in-situ consolidation: a review, J. Compos. Sci. 4 (2020) 149, https://doi.org/10.3390/jcs4040149.
[21] B. Catalog, Wire cloth, wire mesh and woven wire, n.d. http://www.bwire.com/resources.html#how_to_measure_wire_cloth.
[22] A.M. Sastry, Impregnation and consolidation phenomena. https://doi.org/10.1016/B0-08-042993-9/00176-5, 2000.
[23] R.M. Di Benedetto, O.A. Raponi, D.M. Junqueira, A.C. Ancelotti Junior, Crashworthiness and impact energy absorption study considering the CF/PA commingled composite processing optimization, Mater. Res. 20 (2017) 792–799, https://doi.org/10.1590/1980-5373-MR-2017-0777.
[24] A. Deignan, T. Figiel, M.A. McCarthy, Insights into complex rheological behaviour of carbon fibre/PEEK from a novel numerical methodology incorporating fibre friction and melt viscosity, Compos. Struct. 189 (2018) 614–626, https://doi.org/10.1016/j.compstruct.2018.01.084.
[25] N. Vernet, E. Ruiz, S. Advani, J.B. Alms, M. Aubert, M. Barbusrki, B. Barari, J. M. Beraud, D.C. Berg, N. Correia, M. Danzi, T. Delaviere, M. Dickert, C. Di Fratta, A. Endruweit, P. Ermanni, G. Francucci, J.A. Garcia, A. George, G. Hahn, Experimental determination of the permeability of engineering textiles: benchmark II, Compos. Part A. 61 (2014) 172–184, https://doi.org/10.1016/j.compositesa.2014.02.010.
[26] R. Arbter, J.M. Beraud, C. Binetruy, L. Bizet, J. Breard, S. Comas-Cardona, C. Demaria, A. Endruweit, P. Ermanni, F. Gommer, S. Hasanovic, P. Henrat, F. Klunker, B. Laine, S. Lavanchy, S.V. Lomov, A. Long, V. Michaud, G. Morren, E. Ruiz, H. Sol, F. Trochu, B. Verleye, M. Wietgrefe, W. Wu, G. Ziegmann, Experimental determination of the permeability of textiles: a benchmark exercise, Compos. Part A. 42 (2014) 1157–1168, https://doi.org/10.1016/j.compositesa.2011.04.021.
[27] I. Takeda, G. Kalinka, L. Gorbatikh, S.V. Lomov, I. Verpoest, Influence of cooling rate on the properties of carbon fiber unidirectional composites with polypropylene, polyamide 6, and polyphenylene sulfide matrices, Adv. Compos. Mater. 29 (2019) 101–113, https://doi.org/10.1080/09243046.2019.1651083.
[28] M.A. Bashir, Use of dynamic mechanical analysis (DMA) for characterizing interfacial interactions in filled polymers, Solids 2 (2021) 108–120, https://doi.org/10.3390/solids2010006.
[29] M.A. Efroymson, Multiple Regression Analysis, John Wiley & Sons, New York, NY, 1960.
[30] L.S. Aiken, S.G. West, Multiple Regression: Testing and Interpreting Interactions, Sage, Newbury Park, CA, 1991.
[31] G.K. Uyanic, N. Guler, A study of multiple linear regression analysis, Soc. Behav. Sci. 106 (2013) 234–240, https://doi.org/10.1016/j.sbspro.2013.12.027.
[32] H. Akaike, A new look at the statistical model identification, IEEE Trans. Automat. Control 19 (1974) 716–723, https://doi.org/10.1109/tac.1974.1100705.
[33] Z. Wu, J. Li, C. Huang, L. Li, Effect of matrix modification on interlaminar shear strength of glass fibre reinforced epoxy composites at cryogenic temperature, Phys. Procedia 67 (2015) 1068–1073, https://doi.org/10.1016/j.phpro.2015.06.202.